ISSN: 2449 - 0539
BAYERO JOURNAL OF ENGINEERING AND TECHNOLOGY (BJET) VOL. 18 No. 1, JAN 2023 PP 16-31

IMPACT OF CLIMATE CHANGE ON RAINFALL EROSIVITY AND WATER RESOURCES AT CAMERON HIGHLANDS USING ENSEMBLE GCMS

Nuraddeen Mukhtar Nasidi[1]* Nura Jafar Shanono [1] and Muazu Dantala Zakari [1, 2]

[1]Department of Agricultural and Environmental Engineering, Faculty of Engineering, Bayero University, Kano. P.M.B. 3011, Kano – Nigeria

[2] Department of Biological and Agricultural Engineering, Faculty of Engineering, Universiti Putra Malaysia. 43300 Serdang, Selangor Darul Ehsan, Malaysia

*Correspondence: nmnasidi.age@buk.edu.ng

ABSTRACT

Rainfall erosivity is one of the key factors of soil erosion which is expected to change whenever climate variables change and have significant effects on soil conservation policies. It is crucial to identify the future trends of rainfall erosivity and its consequences on water resources in a tropical area where rainfall records are expected to continue to rise. This study aimed to simulate potential precipitations using Global Circulation Models (GCMs), predict erosivity, and determine its impact on water resources in Cameron Highlands. In this study, we used 14 GCMs, AR5 emission scenarios, and two future projection periods. The erosivity factor was determined through the relationship between baseline rainfall intensity and Modified Fournier Index. The result shows a correlation coefficient of 96% between observed and simulated rainfalls. Similarly, the model validation indicated that MAE, SE, and RMSE for the calibrated model are 0.1487, 1.3692, and 1.2499, respectively. The highest rainfall erosivity of 6,039 $MJmmha^{-1}hr^{-1}yr^{-1}$ was projected to occur at the Tanah Rata catchment area located inthe Southwestern part by the 2080s under the RCP8.5 scenario. Also, peak streamflow discharge through Ringlet River is expected to increase by 9.72% up to 110% to reach a peak value in December by 2080s under the RCP8.5 emission scenario. This study revealed a potential increase in rainfall erosivity and corresponding water resources that could be emerged due to climate change which requires appropriate conservation strategies.

Keywords:*Ensemble GCMs; Modified Fournier Index; RCPs; R-factor; Soil Erosion; Spatio-temporal Patterns*

1.0 INTRODUCTION

Nowadays, the impacts of climate change on ecology are considered the most challenging issue confronting the globe (Li *et al*., 2019). Such impacts are raising the global average temperature and high extreme rainfall events. These variations directly affect the erosive power of rainfall and available water resources in a particular watershed. The situation is more pronounced in tropical areas where high extreme weather conditions are expected to keep increasing (Abdullah *et al*., 2019). Rainfall erosivity (R factor) refers to kinetic energy possessed by raindrops and describes the relationship of climatic parameters of rainfall (X. Li & Ye, 2018). Panagos *et al.* (2017) describe rainfall erosivity (R-factor) as the main driving force of soil erosion which has a direct effect on the soil particle detachment. Rainfall erosivity, therefore, indicates the aggressiveness of rainfall to detach soil particles from parent material (Duan *et al.*, 2016). However, soil erosion rate exhibits a non-linear relationship to rainfall erosivity which mainly depends on raindrop sizes,

intensity, and duration of effective rain (Zhao *et al.,* 2017). Although, erosivity may likely increase with the increase in rainfall intensities to create soil saturation and ponding. This will ultimately increase the detachment capacity of the soil particle by the raindrops. The essential characteristics of rainfall are intensity, amount, duration, and frequency which are often influenced by climate change. Thus, rainfall events with high magnitude are likely to have more R-factor and corresponding runoff volume which eventually increase soil determent and sediment transport capacity (Correa *et al.,* 2016).

Erosivity and availability of water resources are expected to vary in response to changes in climate variables. These changes have been directly linked to effects on soil erosion and sedimentation (Neal *et al.*, 2005). In a global context, rainfall patterns vary in time and space with the expected increase in tropical and subtropical areas (Marziali *etal.*, 2017). Previous studies established that tropical climates have a high potential for mean erosivity rise and consequential change in river flows (Amin *et al.*, 2019; de Mello *et al.,* 2015). Moreover, assessing a spatial and temporal variation in erosivity is imperative to establishing a relationship between climate characteristics and soil conservation measures. Thus, it is essential to understand the implications of change in rainfall behavior on soil and water resources. Otherwise, it inspires more potential soil erosion in the future and triggers other serious environmental problems on soil conservation and reservoir plans; such as soil erosion, landslides, flooding, and sedimentation (Razali *et al.,* 2018).

For example, in Cameron highlands, the Ringlet reservoir is an important water resource being used to generate electricity downstream (Teh, 2011). Unfortunately, the runoff water carries large amounts of sediment which are being deposited along the watercourse and finally into the dam. This incident has resulted in a reduced power generating capacity due to sedimentation at the water storage reservoirs (DID, 2012). To maintain a continuous power supply and to improve water quality, continuous daily dredging operations have been initiated along the Ringlet River and the Sultan Abu Bakar dam. Conversely, water resources management has been questioning the agricultural operations at hilly farms for high soil erosion which exacerbates the rate of sediment yields. However, the impact of climate change is another phase that leads to changing rainfall parameters with consequences on soil erosion and sedimentation of the rivers.

Climate change is likely to have a great influence on rainfall erosivity in Malaysia being located in a tropical region and has been reported that studies on change in rainfall erosivity due to climate effects are still inadequate in Southern Asia (Pradhan *et al.,* 2012; Semenov and Stratonovitch, 2010). Therefore, this type of study is highly substantial, particularly in Cameron highlands, because of repeated environmental issues happening in the area such as flooding, soil erosion, sedimentation of rivers, and landslides. Thus, evaluation of rainfall erosivity and its implications on water resources will provide management with information for effective soil and water resources conservation plans. In addition, this will help to prepare in advance and take necessary initiative-taking measures to control soil erosion and over flooding. Unlike most the previous works, this study used 20 ensemble GCMs for enhanced projections to ensure a considerable degree of accuracy (Abdullah *et al.*, 2018). The result of this study can reflect the relative changes to be expected in other parts of the world with similar climatic conditions not necessarily narrowed to the study area.

Consequently, the objective of the study was to assess the climate change impacts on rainfall erosivity and water resources at Cameron Highlands using ensemble GCMs. The process employs a multiplicative delta change method for downscaling the climate data to a local scale for the impact assessment. All the emission scenarios available in the Fifth Assessment Report (RCP2.6, RCP4.5, RCP6.0, and RCP8.5) are applied for the study.

2.0 MATERIALS AND METHOD

2.1 Study Area

Cameron Highlands is located at the Pahang of Peninsular Malaysia situated on 4˚28'N, and 101˚23'E geographic coordinates with average temperatures of 24^{o}C and 14^{o}C during the day and night, respectively. The elevation ranges between 543 m and 1667 m above mean sea level with average annual precipitation of 2660 mm (Abdullah *et al*., 2019; Razali *et al.,* 2018). This region has two distinctive peaks periods of monthly rainfall amounts with the first peak rainfall observed in April while the second with higher rainfall volume in November (Teh, 2011; Shanono *et al.* 2019). These highlands are regarded as a vital hill station for the country which occupies an area of 712.18 square kilometers. The area is surrounded by Kelantan and Perak from north and west respectively and has a potential for growing a wide variety of vegetables, flowers, and other ornamental plants. The excellent climatic condition in the highlands provides an opportunity for agricultural activities as the main business and attracts many tourists (Gasim *et al.,* 2012; Razali *et al.,* 2018).

2.2 Global Circulation Models and Future Scenarios

In this study, the GCMs data were accessed from the World Climate Data Center (https://cera-ww.dkrz.de/ WDCC/ui/cerasearch) under the Fifth Assessment Report (AR5) of the Intergovernmental Panel on Climate Change (IPCC). The projections were conducted under four emission scenarios; RCP2.6, RCP4.5, RCP6.0, and RCP8.5 obtained from the IPCC. This represents low, medium, high, and very high greenhouse gas emission levels respectively (Abdullah *et al.,* 2018). In addition, the data source contains GCMs outputs of the Coupled Model Intercomparison Project Phase 3 (CMIP3) archive with both historical and future projected climate data on a global scale (Table 1). In this study, thirty years of historical data (1976–2005), is defined as baseline climate while the multiplicative delta change statistical method was applied for bias correction. Moreover, the downscaled GCMs data was achieved to approximately 1.0 km^2 resolution local scale on-site daily precipitation datasets for the impact assessment.

Table 1. Atmospheric Global Circulation Models(GCMs)

Institution	Country	GCM Name	Resolution
Commonwealth Scientific and Industrial Research Organization/ Bureau of Meteorology.	Australia	ACCESS1-3	$1.25^o \times 1.87^o$
Beijing Climate Center, China Meteorological Administration	China	BCC-CSM1-1	$2.78^o \times 2.81^o$
National Center for Atmospheric Research.	USA	CESM1-BGC	$0.9^o \times 1.25^o$
Centro Euro-Mediterraneo sui CambiamentiClimatici.	Italy	CMCC-CMS	$1.9^o \times 1.9^o$
EC-EARTH consortium published at Irish Centre for High-End Computing.	Netherlands	EC-EARTH	$1.12^o \times 1.12^o$
NASA/GISS (Goddard Institute for Space Studies).	USA	GISS-E2-R	$2^o \times 2.5^o$
Russian Institute for Numerical Mathematics Climate Model.	Russia	inmcm4	$1.5^o \times 2^o$
Institute Pierre-Simon Laplace.	France	IPSL-CM5A-LR	$1.89^o \times 3.75^o$
Bjerknes Centre for Climate Research, Norwegian Climate Center.	Norway	NorESM1-m	$1.89^o \times 2.5^o$
Canadian Centre for Climate Modeling and Analysis.	Canada	CanESM2	$2.8^o \times 2.8^o$
NOAA Geophysical Fluid Dynamics Laboratory.	USA	GFDL-ESM2G	$2.05^o \times 2^o$
NOAA Geophysical Fluid Dynamics Laboratory.	USA	GFDL-ESM2M	$2.5^o \times 2^o$
Meteorological Office Hadley Center.	Canada	HadGEM2-CC	$1.88^o \times 1.25^o$
Meteorological Office Hadley Center.	Canada	HadGEM2-ES	$1.88^o \times 1.25^o$

2.3 Downscaling of GCMs by Change Factor Method (CFM)

This method entails several steps to estimate the empirical cumulative distribution functions (CDFs) for future GCM (GCM_f) and baseline (GCM_b) for all the emission scenarios (Matonse *et al.,* 2011; Shah *et al.,* 2019). In the CFM additive method, the arithmetic difference between a GCM variable derived from a current climate simulation with that derived from a future climate scenario at the same GCM grid location is calculated. This difference is then added to the local values observed to produce the future model simulations. This method is typically suitable for downscaling the temperature. However, for the derivative of precipitation, a multiplicative change factor (MCF) was introduced to increase the accuracy of downscaling (Matonse *et al.,* 2011).

MCF is calculated in the same method except that the ratio of future to present GCM simulations is multiplied rather than the arithmetic difference. That is, the observed values are then multiplied by the CF instead of adding. This method assumes that the GCM produces a reasonable estimate of the relative change in the value of a variable and is typically used for downscaling the precipitation GCMs data. The method for calculating a single CF is that the first stage is to compute the mean values of GCM simulated baseline and future climates using Equations 1 and 2. Secondly, the multiplicative change factors (CFmul) were calculated using Equation 3, and lastly, to obtain local scaled future values (LSf,i) using Equation 4 Abdullah *et al.,*(2018).

$$\overline{GCM} = \sum_{i=1}^{nb} \frac{GCM_{b,i}}{n} \qquad (1)$$

$$\overline{GCM} = \sum_{i=1}^{nf} \frac{GCM_{f,i}}{n} \qquad (2)$$

$$CF_{mul} = \frac{\overline{GC\ \ f}}{\overline{GCM_b}} \quad (3)$$

$$LS_{f,i} = LO_l \times CF_{mul} \quad (4)$$

Where GCM_b and GCM_f represent the values from a GCM baseline and GCM future climate scenario, respectively. $\overline{GCMb}$ and $\overline{GCMf}$ are the mean values from a GCM baseline and GCM future scenario for the designated temporal domain,nb and nf are the number of values in the temporal domain of the GCM baseline and GCM future scenario. LOb_iisthe observed values of the meteorological variable (at the i^{th} time interval) at an individual meteorological station. LSf_{mul} is the value of future scenarios of the variable obtained using a multiplicative formulation of CFM.

2.4 Weighted Means Ensemble of GCMs

Many recent studies recommended the use of ensemble means of GCMs for climate projection studies as a way forward to improve projection accuracy e.g. (Amanambu *et al.*, 2019; Panagos *et al.*, 2017; Pheerawat and Udmale, 2017; Zhao *et al.,* 2017). It is believed that this approach ensures a minimum level of uncertainty inherently possessed by the global models. Since, each GCM can project different future climate variables, which indicates the gross uncertainty associated with the climate models (Buytaert *et al.,* 2010). Thus, it is universally agreed that weighted ensemble means can help to make stronger projections taking into consideration, the contribution of each model studied. In this study, the weight given to each GCM was based on the mean deviation between simulated and observed monthly values of precipitation from the baseline period. Therefore, GCMs with greater weight predict climatic values with more accuracy in the future. Equation 5 was used for weight determination as presented by Abdullah et al., (2018)which was applied to each climate model's scenario.

$$W_i = \frac{\left(\frac{1}{\Delta P_{i,j}}\right)}{\sum_{j=1}^{n}\left(\frac{1}{\Delta P_{i,j}}\right)} \quad (5)$$

Where, W_i is the weight of each model in a month i and ΔP_{ij} is the difference between the average of precipitation simulated j in a month i of the baseline period (1976-2005) from the corresponding observed data in the same period.

To establish climate change scenarios, Equations 6 was applied to the average of 30 years future periods; (2040-2069) and (2070-2099) for each climate model and its corresponding simulated baseline period (1976–2005). Also, to generate mean weighted ensemble GCMs, Equation 7 was applied to the scenario files with different GCMs and emissions,i.e., RCP2.6, RCP4.5, RCP6.0, and RCP8.5.

$$P = \frac{\overline{P}_{GCM_{f,i}}}{\overline{P}_{GCM_{b,i}}} \quad (6) \qquad E = \sum_{j=1}^{n} P_{i,j} \times W_{i,j} \quad (7)$$

Where; Pi is climate change scenarios related to precipitation for a month i (1<i<12); $\overline{P}$ is the simulated future and historical average precipitation of 30 years, derived from each climate model for a month I, $P_{i,j}$,and $W_{i,j}$ are obtained from Equations 5 and 6, n is the number of climate models, and E represents the mean ensemble GCMs.

2.5 Rainfall Erosivity (R-factor)

As a numerical index, the R-factor describes the aggressiveness of rainfall events to erode soil particles from their initial location (Gericke *et al.,* 2019). This factor is directly influenced by changes in precipitation pattern and the evaluation of these changes is computed on monthly and yearly bases. There are several methods available for estimating R-factor which utilize different rainfall record series. Some methods used both annual and monthly rainfall data while some used total annual data (Liu *et al.,* 2018). In this study, a method proposed by Renard and Freimund(Renard and Freimund, 1994) was used for

calculating R-factor based on an empirical relationship between rainfall intensity and Modified Fournier Index (MFI). The MFI provides information on climatic aggression to dislocate soil particles and it has been correlated with the amount of soil washed by surface runoff (Renard and Freimund, 1994). MFI has been calculated from both monthly and annual rainfalls data using Equation 8, and the R factor was then computed from Equations 8 and 9, respectively. Many studies confirmed that there is a strong correlation between intensity and corresponding MFI for the same month of rainfall (Arnoldous, 1977) and thus, we applied MFI to compute the R-factor.

$$MFI = \frac{\sum_{i=1}^{12} p_i^2}{P} \quad (8)$$

$$R = 95.77 - 6.081F + 0.477F^2 \quad (9)$$

Where Pi is the average monthly rainfall (mm) for month i, P is the mean annual precipitation (mm), R is the erosivity factor in MJmmha^{-1}hr^{-1}yr^{-1} and F represents the MFI.

2.6 Stream Flow Measurements

The rate of stream outflow directly depends upon both amounts of rainfall received by the watershed and retentions by abstractions. In hilly areas, topography and drainage density play significant roles in the behavior of the outflow hydrograph. However, farming operations in hilly regions create excessive soil disturbance and encourage more sediment movements downstream(Nasidi *et al.,* 2020b). Similarly, the volume of runoff generated from such locations is enormous and requires appropriate measures to manage at non-erosive velocity. In this study, due to the limited availability of data for the complete year calendar, we used streamflow data provided by the department of irrigation and drainage, Malaysia(Nasidi et al., 2020a). The dataset constitutes daily, and sub-daily streamflow recorded for fifty-five years durations. Thus, the corresponding periods of rainfall data were extracted for performance testing.

2.7 Validation of the Ensemble Model

The performance evaluation of the downscaled ensemble GCMs was conducted by assessing four indexes of performance as Standard Error (SE), Root means square error (RMSE), and Mean Absolute Error (MAE). The evaluation process includes the measurement of the difference between observed and simulated local variables (precipitation) at each station of the study area. (Equations 10 to 12)

$$SE = \sqrt{\frac{\sum\left(y_{obs} - y_{sim}\right)^2}{n-k-1}} \quad (10)$$

$$MAE = \frac{1}{n}\sum\left|y_{obs} - y_{sim}\right| \quad (11)$$

$$RMSE = \sqrt{\frac{\sum\left(y_{obs} - y_{sim}\right)}{n}} \quad (12)$$

Where Yobs is the observed data, Ysim, is the simulated data, n is the number of recorded data in the validation dataset and k is the number of independent variables in the modeling processes.

3. RESULT AND DISCUSSION

3.1 Calibration and Validation of the Ensemble GCMs

In this study, the period of precipitation datasets used are historical (1976-2005) and future projections (the 2050s and 2080s). Simulation of rainfall was accomplished using the change factor statistical regression method and the performance assessment of the modeled data was achieved by comparing the simulated precipitation with observed datasets for the same period. The outcome revealed that MAE, SE, and RMSE for the calibrated model are 0.1487, 1.3692, and 1.2499, respectively. Moreover, fifteen

years of observed mean daily precipitation data (2005-2019) was used for the validation purpose due to limited observed data in some stations. This was then, correlated with the same period of simulated GCMs data with a correlation coefficient of 96% (Figure 1a). During the validation period, the highest mean daily precipitation of about 18.6 mm was recorded for both simulated precipitations. This relationship demonstrates a good distribution pattern of rainfall for the period of performance assessment. Thus, the performance of this model during the testing period shows its capability to predict future precipitation with high certainty.

Secondly, the study compared observed maximum daily streamflow discharge with daily precipitation records, assuming that, it will produce a direct relationship (Figure 1b). The correlation coefficient of 0.44 indicates a strong correlation between the observed streamflow and precipitation on monthly basis. Moreover, shows that the Ringlet stream flows at a peak discharge of 5.8 m^3/s during November, December, and January. It could also note that, in all the months of the year, values of rainfall exceed the streamflow except in January, where it could be due to excess runoff from the preceded months.

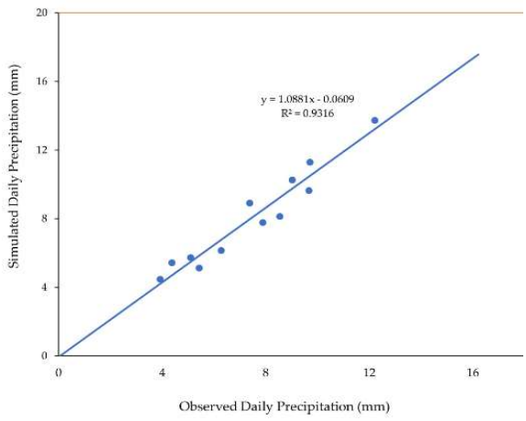

(a)

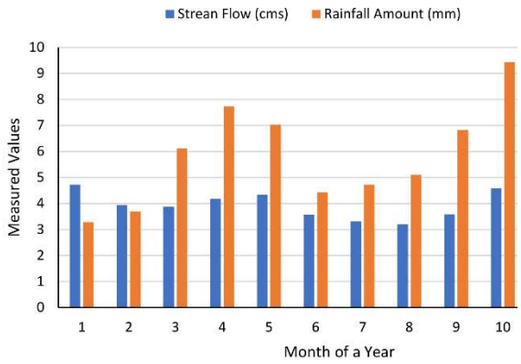

(b)

Figure 1. (a) Validation of GCMs data (b) Comparing Annual Precipitation with Stream flow at Ringlet River Outlet.

3.2 Projection of Mean Monthly Precipitation and Stream Flow

In this study, the multi-model ensemble GCMs project future rainfall variations in two periods of the same length within the 21st century. The periods are representing medium-term (2040-2069) and long-term (2070–2099) respectively. The study refers to 2040-2069 as the 2050s and the 2070–2099 period as the 2080s for simplicity. All the future scenarios were studied at a mean monthly based scenario because GCMs daily projections were transformed into 30-year mean monthly and compared with observed measurements during the same period. The weighted average of the ensemble means of 14 GCM projections aims to provide an average change of the rainfall distribution patterns projected at the Cameron Highlands.

Figure 2 demonstrates the change in rainfall distribution patterns for the 2050s period predicted under four emission scenarios. In this period, the amount of projected rainfall for all the emission scenarios has increased to about 30% relative to baseline conditions. However, there are no considerable changes found among the scenarios in June and September. Conversely, there is a noticeable increment of projected rainfall volumes particularly in both November and December where the ensemble GCMs predicted in the range of 9% and 20% increments, respectively. Moreover, during March, changes in projected rainfalls were observed under the emission scenarios, except that RCP4.5 and RCP6.0 have nearly the same projection patterns. However, decreases in projected rainfalls were experienced during amounts June and July particularly under all the RCPs except RCP6.0 scenarios. For instance, in June, the

ensemble GCMs model projects rainfall of -12% and -6% under RCP8.5 and RCP4.5 relative to baseline climate, respectively. Generally, the projected rainfall amount has considerably increased from the baseline condition for all the scenarios and two projection periods.

In the 2080s projection, the ensemble model predicts substantially more rainfall distribution patterns when compared to the 2050s projection, where all the scenarios projected the volume of rainfall above the baseline (Figure 3). Except that, the decreasing trends were observed in July where -5% future rainfall was recorded relative to baseline under the RCP4.5 scenario. In this period, we found that there are more distinctive variations of projected rainfalls among the emission scenarios, for example, there are 10%, 29%,48%, and 55% more rainfall in January under RCP2.6, RCP4.5, RCP6.0, and RCP8.5 relative to baseline climate, respectively. The pattern of projected rainfall reveals two peak volumes like that of the baseline condition. Although all the scenarios produced different rainfall amounts, there exist overlaps in some months, for instance, in June and July. However, it is observed that the RCP2.6 scenario projects almost the same rainfall as RCP4.5 for both medium-term and long-term periods. This can be explained by the fact that; the RCP2.6 scenario assumes that stringent measures are applied in the release of greenhouse gases which is a factor responsible for climate variability.

Another noticeable change in rainfall amount occurs during October and November when all the scenarios produced distinctly high rainfall amounts. RCP8.5 scenario projects a high volume of rainfall of more than 20% from baseline which may be unsafe unless adequate measures are put in place. Furthermore, there is a slight and continuous shift of rainfall peak from April to November in all the scenarios from the 2050s to 2080s. This is an important observation that peak rainfall in November is expected to continue to increase while the second peak rainfall period (April) will be diminishing. Hence, there may be more concentrated rainfall volume toward the end of each year (in October and November) than in the other months of the year. This reveals an increasing trend of potential soil erosion due to climate change and could be more severe toward the end of the 21st century.

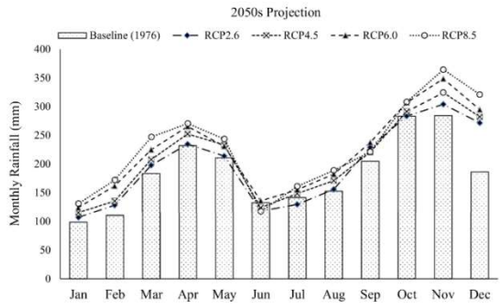

Figure 2. Projected Rainfall in the 2050s under Emission Scenarios

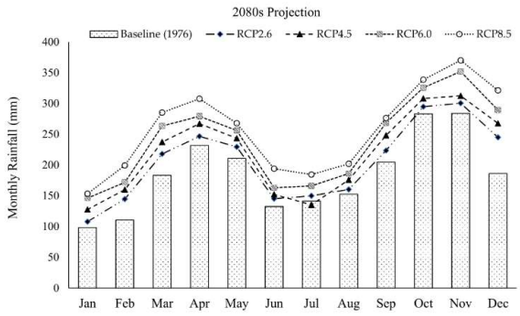

Figure 3. Projected Rainfall in the 2080s under Emission Scenarios

3.3 Projection of Future Stream Flows

Calibration and validation of river flow discharges are the ultimate product of the physical hydrology system coupled with the local climate model. It reveals consistent stream discharge hydrographs in the watershed when compared to the corresponding observations. Figure 4 shows simulated monthly stream flows, observed rainfall, and baseline streamflow in the 2050s period. It revealed that there is proportional changes between observed and simulated stream flows for both the projection scenarios. In January, there is an 8.7%, 17.2%, 26.1%, and 33.2% increase in streamflow for RCP2.6, RCP4.5, RCP6.0, and RCP8.5 scenarios relative to baseline, respectively. Similarly, the highest flow is observed from November to December with ranged values from 24% to 106% under RCP2.6 and RCP8.5 scenarios correspondingly. Moreover, some months show decreasing streamflow, for example, June and July with considerably lower stream discharges of -32% relative to the baseline condition.

Similarly, the observed streamflow, observed precipitation and the projected stream flows in the 2080s period are presented in Figure 5. In this period,

there is a considerable increase in projected streamflow for the 2050s period and relative baseline. Also in January, there is a 9.7%, 29.8%, 48.6%, and 55.8% increment in-stream sizes compared with baseline climate for respectively RCP2.6, RCP4.5, RCP6.0, and RCP8.5 scenarios. However, the extreme flow volumes appeared at both the beginning and end of the year. The total range values of increased stream size are from 9.72% to 110% for the scenarios. Nevertheless, there is one month (June) with relatively lower streamflow than the baseline condition of streamflow by 3% under the RCP2.6 scenario.

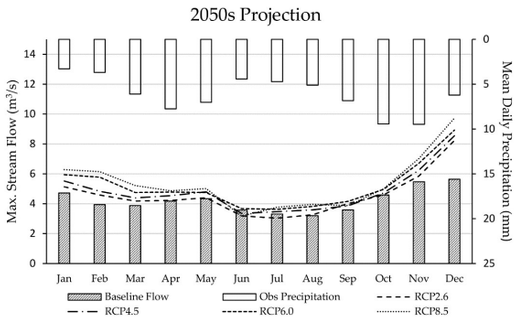

Figure 4. Projected Stream Flows in 2050s

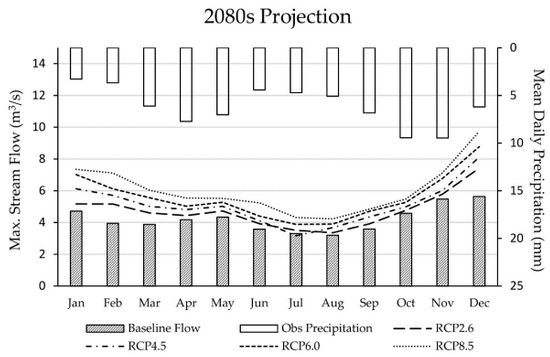

Figure 5. Projected Stream Flows in the 2080s

3.4 Future Projections of Rainfall Erosivity

In this study, the simulated climate ensemble model projects R-factor for the 21st century under AR5 emission scenarios (Figure 6). The result indicates that the simulated global climate model is capable of producing temporal and annual spatial patterns of the erosivity. All the scenarios produced distinctively different projections of rainfall erosivity depending on the projection period and emission scenario. In the 2050s under the RCP2.6 scenario, the spatial projection of the R-factor is found highest of 4,599 $MJmmha^{-1}hr^{-1}yr^{-1}$ at Raja with a corresponding lowest value of 2,842 $MJmmha^{-1}hr^{-1}yr^{-1}$ occurs at K.gHabu sub-catchments. Figure 6(b) presents R-factor under RCP4.5 scenarios with similar spatial distribution patterns. RCP6.0 scenario shows more concentrated higher erosivity at LadangTeh with entirely different distribution patterns over the entire watershed. Similarly, the concentration of rainfall erosivity is closely similar in spatial variation under RCP8.5 except that, a maximum R-factor of 5,609 $MJmmha^{-1}hr^{-1}yr^{-1}$ was attained under the RCP8.5 scenario (Figure 6d). Moreover, for all the scenarios considered for the 2050s projection, the range of highest erosivity is from 4,824 to 5,609 $MJmmha^{-1}hr^{-1}yr^{-1}$ respectively.

However, low rainfall erosivity is consistently projected to occur inthe lower part of the study area as shown by the spatial distribution pattern in Figure 7. This could be attributed to low elevation compared to other high-altitude regions within the catchment. There is a noticeable increase of the R-factor relative to both the RCP2.6 scenario and baseline climate. It could also be noted that there is a shift in the spatial distribution of peak erosivity from Raja to Tanah Rata. Similarly, there is a continuous spatial rise of erosivity in the 2050s occurring inthe North-Western part of the study area under RCP6.0 and RCp8.5 scenarios. This is understandable since both RCP6.0 and RCP8.5 represent high greenhouse gas emissions and are expected to produce relatively more variations in climate variables. Nonetheless. This study shows consistently low erosivity at both Southwestern and Northeastern regions of the Catchment, particularly at Kg. Habu where R-factor of about 3,000 $MJmmha^{-1}hr^{-1}yr^{-1}$ was observed under the RCP6.0 scenario. In the 2080s projection period, the spatial distribution pattern shows a remarkably increased concentration of potential erosivity for all the emission scenarios (Figure 7). In the RCP2.6 scenario, the range of projected R-factor is from 3,246 to 5,356 $MJmmha^{-1}hr^{-1}yr^{-1}$ which is relatively far above the 2050s projection. The concentration of erosive rain is more inthe far South-Eastern region and decreases down the south and southwestern regions for all the RCP8.5 scenarios. It is afterward, spreads across the entire North and North-Eastern regions except LadangTeh. Similarly, in the RCP4.5 scenario, the spatial distribution shows more concentration of R-factor at Kg. Raja, and Tanah Rata regions, although, with the difference in the area coverage. Also, the erosivity exhibits uniquely different patterns under the RCP6.0 scenario where both East and West significant R-factor up to 6,210 $MJmmha^{-1}hr^{-1}yr^{-1}$. The regions most affected by this high erosivity are Kg. Raja and LadangTeh. However, the corresponding low rainfall

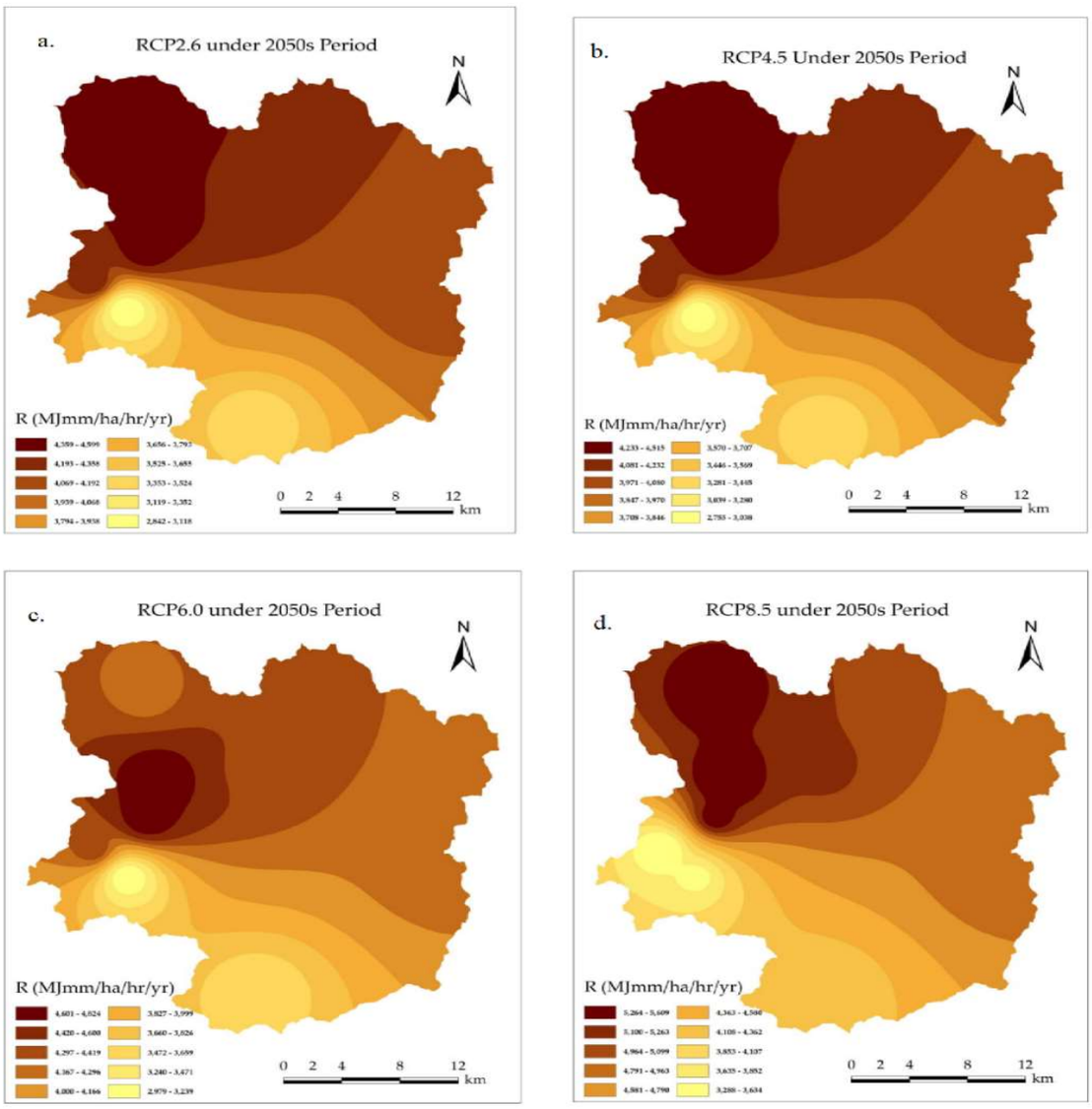

Figure 6. Rainfall Erosivity by 2050s (a) RCP2.6 (b) RCP4.5 (c) RCP6.0 and (d) RCP8.5 Scenarios

Figure 7(d) presents a spatial projection of erosivity under the RCP8.5 scenario and demonstrations consistency with respect to 2050s projected period under the same scenario. For example, Kg Raja in the South-Western region had experienced the highest erosivity (6,292 $MJmmha^{-1}hr^{-1}yr^{-1}$) like in 2050s projecting under the same emission scenario. Similarly, the erosivity projection under RCP6.0 scenario erosivity of 3,956 to 4,288 $MJmmha^{-1}hr^{-1}yr^{-1}$ were observed dawn the Southeast and Southern catchment area.

reveals uniformity in spatial patterns. That is for both 2050s through 2080s projection periods, the predicted erosivity takes similar spatial patterns under RCP6.0 for both East and Western regions. Nonetheless, the general spatial characteristics of erosivity patterns indicated consistency in the spatial distribution patterns for emission scenarios along the projection line. For instance, in the 2050s under RCP2.6 scenario, the spatial pattern of erosivity shows an identical spatial pattern in the 2050s and 2080s periods with a 16% increase. Subsequently, RCP4.5, RCP6.0, and RCP8.5 scenarios have relatively shownan increase in the R-factor from the 2050s to 2080s periods of 12%, 13%, and 28% respectively. This could be attributed to the influence of other environmental factors like topographic effects, atmospheric wind circulation, and other environmental factors.

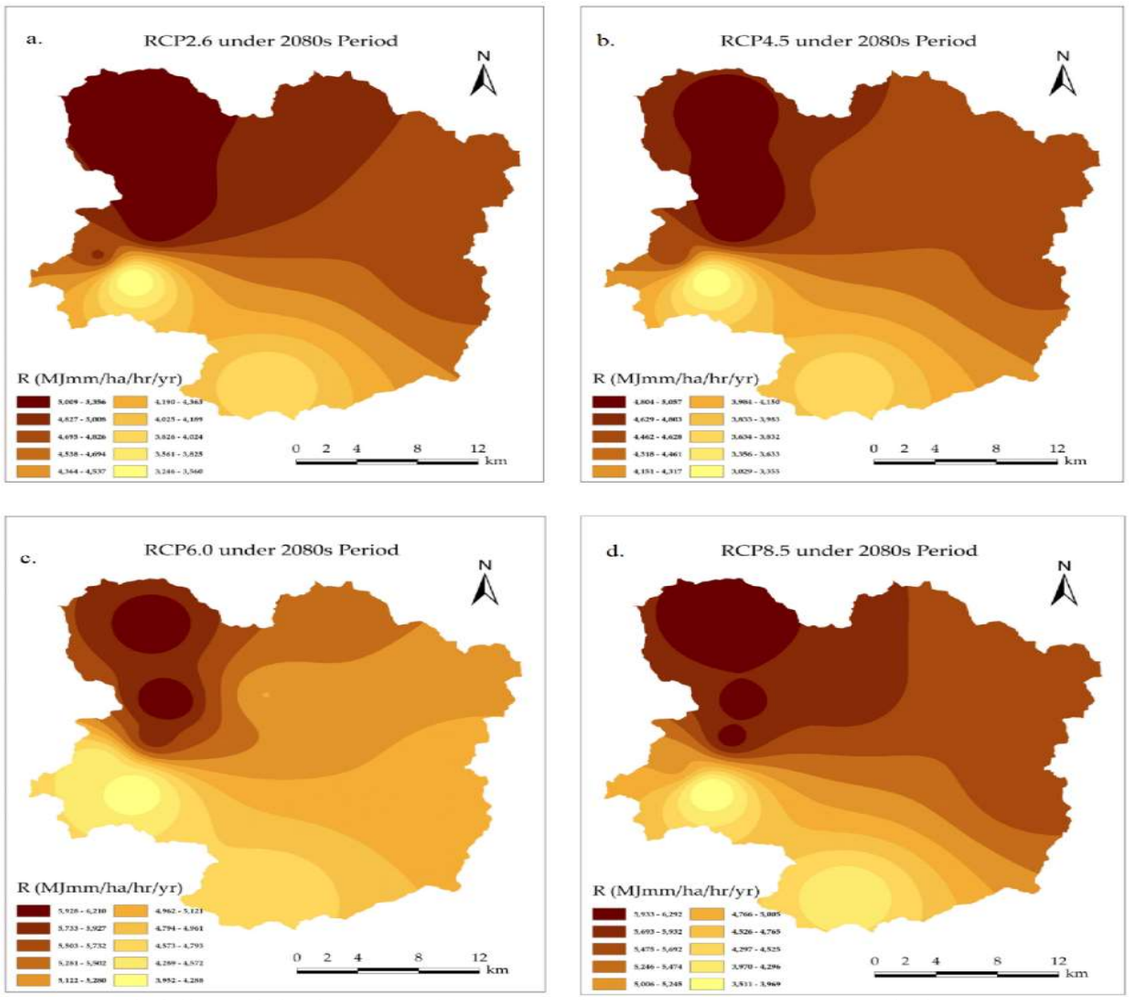

Figure 7. Rainfall Erosivity by 2080s (a) RCP2.6 (b) RC P4.5 (c) RCP6.0 and (d) RCP8.5 Scenarios

3.5. Rainfall Erosivity Variation Relative to Baseline Period

This study compares projected erosivity under four emission scenarios with baseline climate conditions. It clearly shows the relative changes of the erosivity under a given future scenario and projection

timescale. Table 3 illustrates the change in erosivity from baseline at various hilly stations within the Cameron Highlands. It could be observed that there are positive changes in erosivity in all the stations. This translates to that, there is more likely to have high soil erosion in the future at the Cameron Highlands because of increasing rainfall erosivity due to climate change. The erosivity is found to increase with increase in both projection periods and emission scenarios as discussed earlier. This was expected because, there is increasingly higher radiative forcing from RCP2.6 to RCP8.5 emission scenarios. This increment of R-factors is much greater when compared to lower RCPs, which are RCP2.6, RCP4.5, and RCP6.0 scenarios. However, the values of erosivity observed at Tanah Rata and MARDI hill stations with positive erosivity changes relative to the baseline were 33% and 37% by 2050s and 2080 Projection periods, respectively.The increasing trend of rainfall amounts and patterns can reflect the effect of climate change on future rainfall erosivity. Though, increment of rainfall aggressiveness indices should not be viewed directly as an increase in soil erosion. Since, the process is related not only to rainfall factors but also to the dynamics of vegetation, soil properties, and landscape geophysics (Amanambu *et al.*, 2019). Rapid forest shrinkage, particularly due to population pressures and unsustainable use of resources, could play a significant role in exacerbating erosion levels (de Mello *et al.,* 2015). In this study, the projected rainfall erosivity ranged from 2,842 $MJmmha^{-1}hr^{-1}yr^{-1}$ in 2050s to 6,292 $MJmmha^{-1}hr^{-1}yr^{-1}$ in 208s Periods. This projection is consistent with the existing studies conducted for the 21st century in tropical areas globally. This result is as well, in line with the assertion that tropical areas are more likely to experience higher rainfall erosivity (Abdullah *et al.,* 2018). Although, some studies, for example Fanta (Mondal *et al.,* 2016) and Fagbohun*et al*. (Fenta *et al.,* 2017) reported both increase and decrease in rainfall erosivity in some tropical areas.

However, previous studies indicated positive trends of increasing rainfall erosivity in tropical areas in the world. Our study presents the future projection of rainfall erosivity up to 113% in November relative to baseline climate. Mello *et al.,*(2015) reported an increase in potential rainfall erosivity of 49% comparative to baseline in South-Western regions of Brazil. Similarly, Pheerawat&Udmale, (Pheerawat and Udmale, 2017) projected erosivity using three GCMs and two emission scenarios at UdonThani province of North-East Thailand. The results revealed a significant increase in erosivity of 82.6% abouta baseline, where it recorded erosivity up to 15,159 $MJmmha^{-1}hr^{-1}yr^{-1}$ by the end of the 2090s. Moreover, their study compared erosive patterns in the 2030s, 2050s, and 2090s and found that there is an increasing trend like the current study. This could be explained, however, by the structure of the emission scenarios that, the radiative forcing level in the RCP4.5 scenario reaches its peak in about 2060 and stabilizes afterward, while it continues to rise in the RCP8.5 scenario (Pheerawat and Udmale, 2017). Therefore, RCP8.5 is expected to project more severe changes than other scenarios and it happened as expected. Therefore, projected changes in rainfall amount by the model under RCP8.5 are more pronounced than in the remaining scenarios.

Furthermore, Fenta *et al.,*(2017) reported a 59% increase in rainfall erosivity in Eastern Africa with R-factor values of 7,000 MJmmha-1hr-1yr-1 and beyond. Although, few areas were having a decreasing trend. Furthermore, a study conducted by Yang and Lu, (2015) presented a significant increase in rainfall erosivity (17.4%) relative to baseline in Southeastern China during the past half-century. Likewise, the studies conducted by Li and Ye, (2018). Also,Zhao *et al*. (2017) revealed an increasing spatial variation of erosivity trend in Guangdong Province, southern China from 1960 – 2011.

Nonetheless, the projection of considerably high rainfall erosivity is common in a tropical climate., (Amanambu *et al., 2019)* reported erosivity values ranging from 9,976 to 12,627 $MJmmha^{-1}hr^{-1}yr^{-1}$ due to high rainfall intensity in the tropical region of Africa. Panagos *et al.*, (2017) estimated 857 $MJmmha^{-1}hr^{-1}yr^{-1}$ as mean annual erosivity in Europe by 2050 which accounts for about an 18% increase from baseline climates. However, Fagbohun *et al.*, (2016) estimated low erosivity ranged from 3,800 to 4,500 $MJmmha^{-1}hr^{-1}yr^{-1}$ in the tropical area of Africa using GIS-based techniques. The present study discloses potential erosivity changes using multi-model ensemble GCMs under multi-emission scenarios. Meanwhile, it projects reasonably high erosive power of rainfall for two timescales. This contribution can be replicated not only in the study location but in any other places with similar climatic conditions.

4. CONCLUSION

In this study, the rainfall erosivity and water resources were simulated based on the global climate change models using multi-model ensemble means. First, historical and projection precipitation datasets contained in twenty GCMs were extracted from the world climate data center, and then, bias-corrected

using the multiplicative delta change statistical method. Thereafter, spatial, and temporal models were developed under emission scenarios and station elevations. The study discloses that both R-factor and streamflow are increasing with an increase in farm elevation. Moreover, there are increasing trends of rainfall erosivity and river flow discharges throughout the 21st century under the A5 projection scenarios. It is noted that increments are more intense toward the end of the century for both R-factor and stream flows. Similarly, the spatial distribution patterns show a consistent increase of erosivity with regular shapes throughoutthe study area. This indicates that there is more likely to have higher soil erosion and sedimentation of rivers in the future considering the increasing trends of the rainfall erosivity and streamflow due to climate change.

5. REFERENCES

Abdullah, A. F., Amiri, E., Daneshian, J., Teh, C. B. S., Wayayok, A., Massah Bavani, A., & Ahmadzadeh Araji, H. (2018). Impacts of climate change on soybean production under different treatments of field experiments considering the uncertainty of general circulation models. *Agricultural Water Management*, *205*(May), 63–71. https://doi.org/10.1016/j.agwat.2018.04.023

Abdullah, A. F., Wayayok, A., Nasidi, N. M., Hazari S. A. F, K., Sidek, L. M., & Selamat, Z. (2019). Modeling Erosion and Landslides Induced by Farming Activities at Hilly Farms. *Jurnal Teknologi*, *6*, 195–204.

Amanambu, A. C., Li, L., Egbinola, C. N., Obarein, O. A.; Mupenzi, C.; Chen, D., Amanambu, A. C., Li, L., Egbinola, C. N., Obarein, O. A., Mupenzi, C., & Chen, D. (2019). Spatio-temporal variation in rainfall-runoff erosivity due to climate change in the Lower Niger Basin, West Africa. *CATENA*, *172*(September 2018), 324–334. https://doi.org/10.1016/j.catena.2018.09.003

Amin, I. M. Z. bin M., Ercan, A., Ishida, K., Kavvas, M. L., Chen, Z. Q., & Jang, S. H. (2019). Impacts of climate change on the hydro-climate of peninsular Malaysia. *Water (Switzerland)*, *11*(9), 1798. https://doi.org/10.3390/w11091798

Arnoldous, H. M. J. (1977). Methodology used to determine the maximum potential average annual soil loss due to sheet and rill erosion in Morocco. *FAO Soil Bulletin*, 39–48. http://www.fao.org/3/a-ar114e.pdf

Buytaert, W., Vuille, M., Dewulf, A., Urrutia, R., Karmalkar, A., & Célleri, R. (2010). Uncertainties in climate change projections and regional downscaling in the tropical Andes: Implications for water resources management. *Hydrology and Earth System Sciences*, *14*(7), 1247–1258. https://doi.org/10.5194/hess-14-1247-2010

Correa, S. W., Mello, C. R., Chou, S. C., Curi, N., & Norton, L. D. (2016). Soil erosion risk associated with climate change at Mantaro River basin, Peruvian Andes. *Catena*, *147*, 110–124. https://doi.org/10.1016/j.catena.2016.07.003

de Mello, C. R., Ávila, L. F., Viola, M. R., Curi, N., & Norton, L. D. (2015). Assessing the climate change impacts on the rainfall erosivity throughout the twenty-first century in the Grande River Basin (GRB) headwaters, Southeastern Brazil. *Environmental Earth Sciences*, *73*(12), 8683–8698. https://doi.org/10.1007/s12665-015-4033-3

DID. (2012). Urban Stormwater Management Manual for Malaysia. In N. A. Zakaria, A. A. Ghani, & C. K. Chang (Eds.), *Manual* (2nd ed.). Department of Irrigation and Drainage (DID) Malaysia.

Duan, X., Gu, Z., Li, Y., & Xu, H. (2016). The

spatiotemporal patterns of rainfall erosivity in Yunnan Province, southwest China: An analysis of empirical orthogonal functions. *Global and Planetary Change*, *144*, 82–93. https://doi.org/10.1016/j.gloplacha.2016.07.011

Fagbohun, B. J., Anifowose, A. Y. B., Odeyemi, C., Aladejana, O. O., & Aladeboyeje, A. I. (2016). GIS-based estimation of soil erosion rates and identification of critical areas in Anambra sub-basin, Nigeria. *Modeling Earth Systems and Environment*, *2*(3), 159. https://doi.org/10.1007/s40808-016-0218-3

Fenta, A. A., Yasuda, H., Shimizu, K., Haregeweyn, N., Kawai, T., Sultan, D., Ebabu, K., & Belay, A. S. (2017). Spatial distribution and temporal trends of rainfall and erosivity in the Eastern Africa region. *Hydrological Processes*, *31*(25), 4555–4567. https://doi.org/10.1002/hyp.11378

Gasim, M. B., Mokhtar, M., Surif, S., Toriman, M. E., Rahim, S. A., & Lun, P. I. (2012). Analysis of thirty years recurrent floods of the Pahang River, Malaysia. *Asian Journal of Earth Sciences*, *5*(1), 25–35. https://doi.org/10.3923/ajes.2012.25.35

Gericke, A., Kiesel, J., Deumlich, D., & Venohr, M. (2019). Recent and future changes in rainfall erosivity and implications for the soil erosion risk in Brandenburg, NE Germany. *Water (Switzerland)*, *11*(5). https://doi.org/10.3390/w11050904

Li, X., & Ye, X. (2018). Variability of rainfall erosivity and erosivity density in the Ganjiang River Catchment, China: Characteristics and influences of climate change. *Atmosphere*, *9*(2). https://doi.org/10.3390/atmos9020048

Li, Y., Xie, Z., Qin, Y., & Sun, Y. (2019). Temporal-spatial variation characteristics of soil erosion in the pisha sandstone area, loess plateau, china. *Polish Journal of Environmental Studies*, *28*(4), 2205–2214. https://doi.org/10.15244/pjoes/92940

Liu, Y. H., Li, D. H., Chen, W., Lin, B. S., Seeboonruang, U., & Tsai, F. (2018). Soil erosion modeling and comparison using slope units and grid cells in Shihmen reservoir watershed in Northern Taiwan. *Water (Switzerland)*, *10*(10). https://doi.org/10.3390/w10101387

Marziali, L., Tartari, G., Salerno, F., Valsecchi, L., Bravi, C., Lorenzi, E., Genoni, P., & Guzzella, L. (2017). Climate change impacts on sediment quality of Subalpine reservoirs: Implications on management. *Water (Switzerland)*, *9*(9), 1–18. https://doi.org/10.3390/w9090680

Matonse, A. H., Anandhi, A., Frei, A., Pierson, D. C., Schneiderman, E. M., Zion, M. S., & Lounsbury, D. (2011). Examination of change factor methodologies for climate change impact assessment. *Water Resources Research*, *47*(3). https://doi.org/10.1029/2010WR009104

Mondal, A., Khare, D., & Kundu, S. (2016). Change in rainfall erosivity in the past and future due to climate change in the central part of India. *International Soil and Water Conservation Research*, *4*(3), 186–194. https://doi.org/10.1016/j.iswcr.2016.08.004

Nasidi, N. M., Wayayok, A., Abdullah, A. F., & Kassim, M. S. M. (2020a). Spatio-temporal dynamics of rainfall erosivity due to climate change in Cameron Highlands, Malaysia. *Modeling Earth Systems and Environment*. https://doi.org/10.1007/s40808-020-00917-4

Nasidi, N. M., Wayayok, A., Abdullah, F. A., & Kassim, M. S. M. (2020b). Vulnerability of Potential Soil Erosion and Risk Assessment at Hilly Farms using InSAR Technology. *Algerian Journal of Engineering*, *02*(2), 44–58. https://doi.org/doi.org/10.5281/zenodo.3841100

Neal, M. R., Nearing, M. A., Vining, R. C.,

Southworth, J., & Pfeifer, R. A. (2005). Climate change impacts on soil erosion in Midwest United States with changes in crop management. *Catena*, *61*(2-3 SPEC. ISS.), 165–184. https://doi.org/10.1016/j.catena.2005.03.003

Nunes, A. N., Lourenço, L., Vieira, A., & Bento-Gonçalves, A. (2016). Precipitation and Erosivity in Southern Portugal: Seasonal Variability and Trends (1950-2008). *Land Degradation and Development*, *27*(2), 211–222. https://doi.org/10.1002/ldr.2265

Panagos, P., Ballabio, C., Meusburger, K., Spinoni, J., Alewell, C., & Borrelli, P. (2017). Towards estimates of future rainfall erosivity in Europe based on REDES and WorldClim datasets. *Journal of Hydrology*, *548*. https://doi.org/10.1016/j.jhydrol.2017.03.006

Pheerawat, P., & Udmale, P. (2017). Impacts of climate change on rainfall erosivity in the Huai Luang watershed, Thailand. *Atmosphere*, *8*(8). https://doi.org/10.3390/atmos8080143

Pradhan, B., Chaudhari, A., Adinarayana, J., & Buchroithner, M. F. (2012). Soil erosion assessment and itscorrelation with landslide events using remote sensing data and GIS: A case study at Penang Island, Malaysia. *Environmental Monitoring and Assessment*, *184*(2), 715–727. https://doi.org/10.1007/s10661-011-1996-8

Razali, A., Syed Ismail, S. N., Awang, S., Praveena, S. M., & Zainal Abidin, E. (2018). Land use change in highland area and its impact on river water quality: a review of case studies in Malaysia. *Ecological Processes*, *7*(1), 19. https://doi.org/10.1186/s13717-018-0126-8

Renard, K. G., & Freimund, J. R. (1994). Using monthly precipitation data to estimate the Rfactor in the revised USLE. *J. Hydrol.*, *157*(1–4), 287–306.

Semenov, M. A., & Stratonovitch, P. (2010). Use of multi-model ensembles from global climate models for assessment of climate change impacts. *Climate Research*, *41*(1), 1–14. https://doi.org/10.3354/cr00836

Shah, S. M. H., Mustaffa, Z., & Yusof, K. W. (2019). Numerical framework to determine instability modes for static vehicles under partial submergence. *International Journal of Integrated Engineering*, *11*(2), 186–194. https://doi.org/10.30880/ijie.2019.11.01.020

Shanono, N. J., Nasidi, N. M., Maina, M. M., Bello, M. M., Ibrahim, A., Umar, S. I., Zakari, M. D., & Putra, U. (2019). *Socio- hydrological study of water users' perceptions on the management of irrigation schemes at tomas irrigation project, kano, nigeria*. *5*(2), 139–145.

Teh, S. H. (2011). Soil Erosion Modeling Using RUSLE and GIS on Cameron Highlands, Malaysia for Hydropower Development [Solborg at Nordurslod]. In *RES | The School for Renewable Energy Science*. https://www.engr.colostate.edu/~pierre/ce_old/Projects/linkfiles/Thesis Soo Huey Teh.pdf

Yang, F., & Lu, C. (2015). Spatiotemporal variation and trends in rainfall erosivity in China's dryland region during 1961-2012. *Catena*, *133*, 362–372. https://doi.org/10.1016/j.catena.2015.06.005

Zhao, Q., Liu, Q., Ma, L., Ding, S., Xu, S., Wu, C., & Liu, P. (2017). Spatiotemporal variations in rainfall erosivity during the period of 1960–2011 in Guangdong Province, southern China. *Theoretical and Applied Climatology*, *128*(1–2), 113–128. https://doi.org/10.1007/s00704-015-1694-5